Optical Engineering

OpticalEngineering.SPIEDigitalLibrary.org

Design studies of varifocal rotation optics

Ingo Sieber
Peter Stiller
Ulrich Gengenbach

SPIE.

Ingo Sieber, Peter Stiller, Ulrich Gengenbach, "Design studies of varifocal rotation optics," *Opt. Eng.* **57**(12), 125102 (2018), doi: 10.1117/1.OE.57.12.125102.

Design studies of varifocal rotation optics

Ingo Sieber,* Peter Stiller, and Ulrich Gengenbach
Karlsruhe Institute of Technology, Institute for Automation and Applied Informatics, Eggenstein-Leopoldshafen, Germany

Abstract. We present the design of a varifocal freeform optics consisting of two lens bodies each with a helical-type surface structure of azimuthally varying curvatures. This arrangement allows for tuning the optical refraction power by means of a mutual rotation of the lens bodies around the optical axis. Thus, the refraction power can be tuned continuously in a defined range. The shape of the helical-type surfaces is formed by a change in curvature subject to the azimuthal angle α. At the transition of the azimuthal angle from $\alpha = 2\pi$ to $\alpha = 0$, a surface discontinuity appears. Since this discontinuity will seriously affect the imaging quality, it has to be obscured. In the initial state, i.e., zero-degree rotation, the curvatures of the opposing surfaces result in a specific refraction power, which is constant over the entire circular aperture. Rotating one of the lens bodies by an angle φ around the optical axis will change the opposing curvatures and result in a change of refraction power. Two circular sectors with different tunable optical refraction powers are formed, thus resulting in a tunable bifocal optics. Obscuring the minor sector will result in a tunable monofocal rotation optics. In contrast to conventional tunable lens systems, where additional space for axial or lateral lens movement has to be allocated in design, rotation optics allowing for a more compact design. A performance analysis of the rotation optics based on simulations is presented in dependence on aperture size as well as approaches to compensate for spherical aberrations. [DOI: 10.1117/1.OE.57.12.125102]

Keywords: freeform optics; varifocal optics; rotation optics; design-for-manufacture.

Paper 181259 received Aug. 31, 2018; accepted for publication Nov. 14, 2018; published online Dec. 6, 2018.

1 Introduction

Generalized, freeform optical elements are lenses with surfaces lacking rotational symmetry. Similar to classical lenses, they affect a light beam by the laws of reflection and refraction at their curved surface structures. Wavelength dependence of the beam shaping is only due to material dispersion. In recent years, freeform optics have been used in many optical applications. This is largely due to the fact that fabrication of freeform surfaces has reached a level at which optical surfaces of good quality can be manufactured by different fabrication processes with sufficiently high accuracy.[1–4] Fields of applications include vehicle lighting[5,6] or beam expanders[7] as well as artistic exhibits,[8,9] or design elements in architecture.[10]

An interesting approach is forming varifocal optics on the basis of freeform optical elements. One example of such optics with tunable refraction power is the principle invented in the 1960's by Luis Alvarez.[11] According to this principle, the refraction power in an optical system consisting of two cubic-type lens parts is varied by mutually shifting both lens parts in lateral direction to the optical axis. Alvarez-lenses were studied extensively[12–14] and proposed for different technical[15–17] as well as ophthalmological applications.[18–22] When using the Alvarez-principle, additional lateral space for lens movement is required in the design. This holds also for conventional lens systems, the refraction power of which can be tuned by mutual shifting of the individual lenses along the optical axis. To prevent additional space requirements, a non-Cartesian tuning motion is needed. The use of mutual rotation for tuning was shown using diffractive optical elements, such as spiral phase plates[23–27] and for refractive optics by using two lens bodies each with a helical-type surface structure of azimuthally varying curvatures.[28–30] The concept of varifocal rotation optics would enable the application of tunable optics in optical systems with severe space limitations. Examples of such optics can be found in ophthalmology, e.g., as optics of an artificial eye[29] or in zoom optics of handheld devices such as, e.g., smart phones or pocket projectors.

This paper presents a simulative performance analysis of the rotation optics in dependence on design parameters. The organization of the paper is as follows: in Sec. 2, the basic principles are developed and a mathematical description of the surfaces is derived. Section 3 shows a simulative performance analysis of the rotation optics and an approach to compensate for spherical aberration. In Sec. 4, an optical simulation and analysis of the rotation optics are performed and results are presented. The paper closes with the conclusions.

2 Basic Principle

In the thin-lens approximation, a rotation angle-dependent refraction power $D(\varphi)$ can be formulated in dependence on the azimuthal change of curvature of the first surface $C_1(\alpha)$ and the second surface $C_2(\alpha, \varphi)$, which will be rotated.

$$D(\varphi) = (n_L - n_0)/n_0[C_1(\alpha) - C_2(\alpha, \varphi)], \tag{1}$$

where n_L is the refraction index of the lens body, n_0 is the refraction index of the ambient medium, α is the azimuth, φ is the rotation angle, and $C = 1/R$.

Choosing a linear dependence of the curvature on the azimuth α, the curvature $C_1(\alpha)$ of the first lens body can be described as a function of α

$$C_1(\alpha) = C_{10} + j_1\alpha, \tag{2}$$

*Address all correspondence to Ingo Sieber, E-mail: ingo.sieber@kit.edu

where $C_1 = 1/R_1$, C_{10} is the curvature at $\alpha = 0$, j_1 is the linear factor of curvature distribution, and α is the azimuth.

Rotating the second lens body, the respective opposing curvature also depends on the rotation angle φ. The equation of the azimuthal curvature distribution $C_2(\alpha)$ hence can be described in dependence on the rotation angle φ:

$$C_2(\alpha) = \begin{array}{ll} C_{20} + j_2(\alpha - \varphi) & \text{for } \varphi \le \alpha \le 2\pi \\ C_{20} + j_2(\alpha - \varphi + 2\pi) & \text{for } 0 \le \alpha < \varphi \end{array}, \tag{3}$$

where $C_2 = 1/R_2$, C_{20} is the curvature at $\alpha = 0$, j_2 is the linear factor of the curvature distribution, α is the azimuth, and φ is the rotation angle.

Equating the linear factors $j_1 = j_2 = j$ and with Eqs. (2) and (3), the angle-dependent refraction power $D(\varphi)$ can be described as

$$D(\varphi) = \begin{array}{ll} \frac{n_L - n_0}{n_0}(C_{10} - C_{20} + j\varphi) & \text{for } \varphi \le \alpha \le 2\pi \\ \frac{n_L - n_0}{n_0}[C_{10} - C_{20} + j(\varphi - 2\pi)] & \text{for } 0 \le \alpha < \varphi \end{array}. \tag{4}$$

Equation (4) means that for every rotation $\varphi \neq 0$ there exist two lens sectors providing a certain refraction power. The difference in refraction power between both sectors, ΔD, is a constant depending on the refraction indices of the materials used and the linear factor j

$$\Delta D = -2\pi j \frac{n_L - n_0}{n_0}. \tag{5}$$

Equation (4) describes the angle-dependent refraction power of a bifocal rotation optics. Obscuration of the "undesired" sector, preferably the smaller sector in the azimuth region $0 \le \alpha < \varphi$, will result in a monofocal optics with tunable refraction power due to a rotation of the second lens body.

Figure 1 shows the shape [(a) 10× exaggerated in height] and contour (b) of a surface were the curvature depends on the azimuth α and, in this example, changes from convex to concave starting at 3 o'clock and proceeding in counterclockwise direction. After a cycle of 2π, a discontinuity appears at the transition from $\alpha = 2\pi$ to $\alpha = 0$.

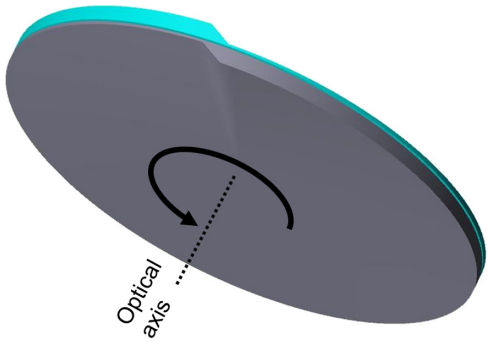

Fig. 2 Rotation optics, consisting of two lens bodies with surfaces of azimuthal curvature dependence in a consecutive arrangement centered and perpendicular to the optical axis. The discontinuity is leveled for manufacturing purposes. The height aspect ratio is unscaled.

Two surfaces of this kind, each constituting a lens body, are needed to form an optics with a rotational tunable refraction power. The lens bodies have to be arranged consecutively and centered around and perpendicular to the optical axis (see Fig. 2). The curvature varies such that lens sectors of two opposing lens bodies will result in the same refraction power over the whole azimuth range in the initial state. Setting the rotation angle φ to zero in Eq. (4) will define the initial setting of the rotation optics: the curvatures of opposed surfaces result in a specific refraction power $D_0 = D(\varphi = 0)$ which is constant over the whole azimuth range (the full 2π sector) and can be defined as the basic refraction power

$$D_0 = \frac{n_L - n_0}{n_0}(C_{10} - C_{20}) \quad \text{for } 0 \le \alpha \le 2\pi. \tag{6}$$

A rotation of one of the lens bodies by an angle φ around the optical axis will change the two opposing curvatures, resulting in a change of refraction power. Two sectors with different tunable optical refraction powers are formed by the mutual rotation, thus resulting in a tunable bifocal optics [see Fig. 3 and Eq. (4)].

Since the discontinuities will seriously affect the imaging quality, they have to be obscured to prevent any disturbing effects in imaging, such as, e.g., scattering. Blocking of only

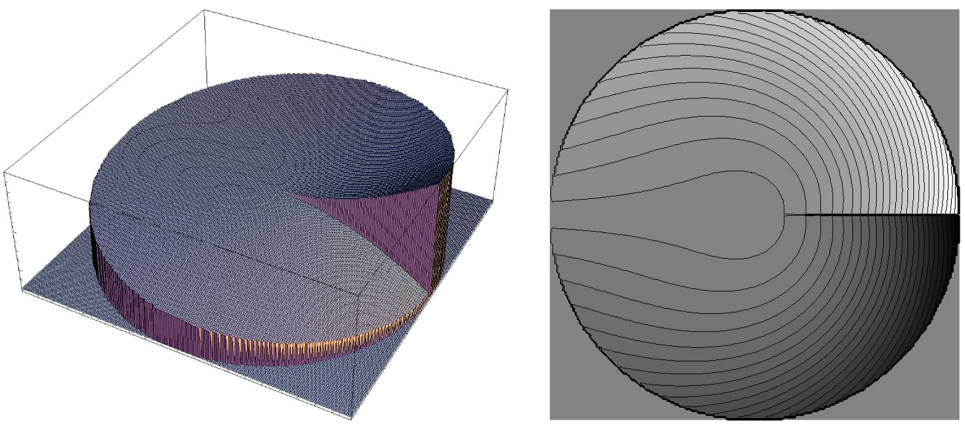

(a) (b)

Fig. 1 (a) Shape and (b) contour of a surface were the curvature depends on the azimuth α. The presentations are 10× exaggerated.

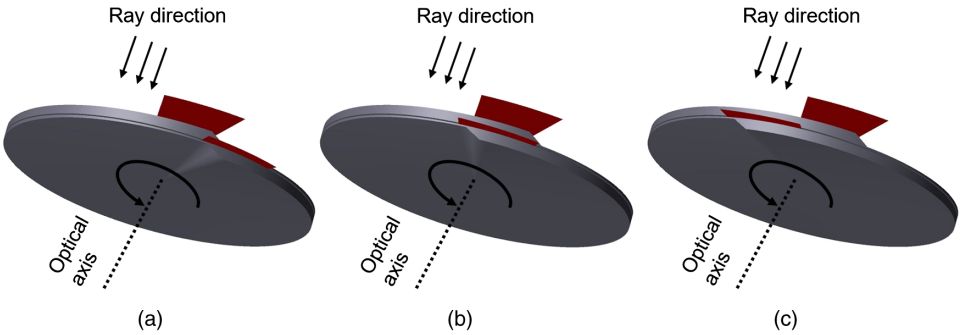

Fig. 3 Rotation optics in different tuned states: (a) $\varphi = 0$ deg, $D = 1$ dpt, (b) $\varphi = 22.5$ deg, $D = 2.5$ dpt, and (c) $\varphi = 45$ deg, $D = 4$ dpt. The discontinuities are obscured as well as the undesired sector in between the discontinuities (for $0 \leq \alpha < \varphi$), thus resulting in a monofocal tunable optics.

a sector of the pupil will not affect the spatial frequency spectrum and hence will not result in a loss of information. Aberrations may be induced by the obscuration and, of course, the obscured energy will not contribute to the image. Figure 3 shows a rotation optics in a tuned state where the second lens body is rotated by an angle $\varphi \neq 0$ around the optical axis. The discontinuities are obscured as well as the undesired sector in between the discontinuities (for $0 \leq \alpha < \varphi$), thus resulting in a monofocal tunable optics.

3 Design and Simulation

To illustrate the design approach, a rotation optics offering a refraction range of three dioptres (dpt) serves as example. The refraction range is motivated by our research in context of the artificial accommodation system, an ophthalmic device designed for restoration of the accommodation ability of the human eye.[31] The range of refraction power is chosen to start at a basic refraction $D_0 = 1$ dpt and to end at a refraction power of $D(\varphi = \varphi_{\max}) = 4$ dpt. The design parameters are listed in Table 1.

The change of curvature with azimuth is shown in Fig. 4 for both surfaces, respectively. The solid line represents the progression of the curvature of the first surface, the dotted that of the second surface. Note that both curves are straight parallel lines, which is because we have chosen a linear approach in calculating the curvature in dependence on the azimuth and we equated $j_1 = j_2 = j$. Also apparent is that both curves have different starting points C_{10} and C_{20}, which has its origin in the fact that the basic refraction power $D_0 \neq 0$. Zero crossings of the abscissa are $\pi/24$ left (front surface) and right (rear surface) of the azimuth value π.

The function of the rotation optics underlies the principle of geometrical optics, where the refraction power is determined by the following equation: $D = (n_L - n_0)/n_0(1/R_1 - 1/R_2)$. Hence, for given refractive indices n_L and n_0, a specific refraction power D can be derived by combining different radii R_1 and R_2, as long as the term $(1/R_1 - 1/R_2)$ stays constant. A variation of the radii with the azimuth following Eqs. (2) and (3) will result in

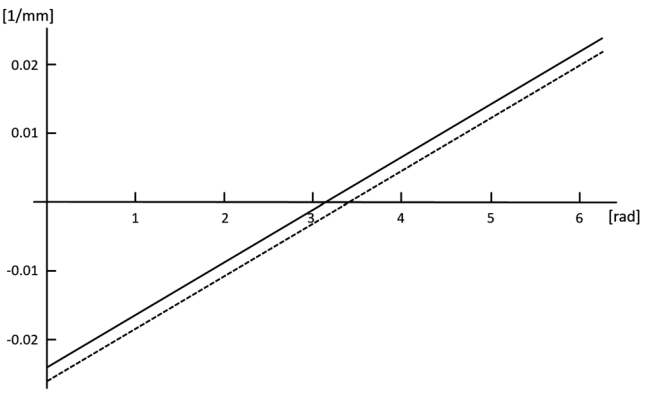

Fig. 4 Change of curvature with azimuth of the first (solid line) and the second (dotted line) surfaces.

an optics with a constant refraction power over the total aperture. But, of course in optical performance there are great differences between the different combinations of radii R_1 and R_2. Figure 5 shows the dependence of the root mean square (RMS) spot radius on the azimuth of the rotation optics in case of zero rotation and a basic refraction power $D_0 = 1$ dpt. Simulation of the RMS spot radii for different profile sections was carried out with Zemax OpticStudio 18.1[32] using spherical lenses with the respective curvatures as references. As insets in Fig. 5, the radii of curvatures of five such lens profile sections in an azimuthal distance of $\pi/2$ are shown scaled by a factor two, to illustrate the change of opposite curvatures. To assign the profile sections to the rotation optics, top of Fig. 5 shows the section lines at the surface of the first part of the rotation optics.

Simulations were conducted using the commercial optical simulation tool OpticStudio by ZEMAX.[32] The helical surfaces were calculated in Mathematica[33] and a 200×200 point cloud was imported to OpticStudio by means of the Grid Sag function. The optical simulation model consists of the rotation optics providing for an amplitude of refraction

Table 1 Design parameters of the rotation optics serving as an example.

D_0	$D(\varphi = \varphi_{\max})$	n_0	n_L	$\varphi_{\max}$	j	C_{10}	C_{20}
1 dpt	4 dpt	1.0	1.5	$\pi/4/4$	7.640 dpt/rad	−0.0231/mm	−0.0251/mm

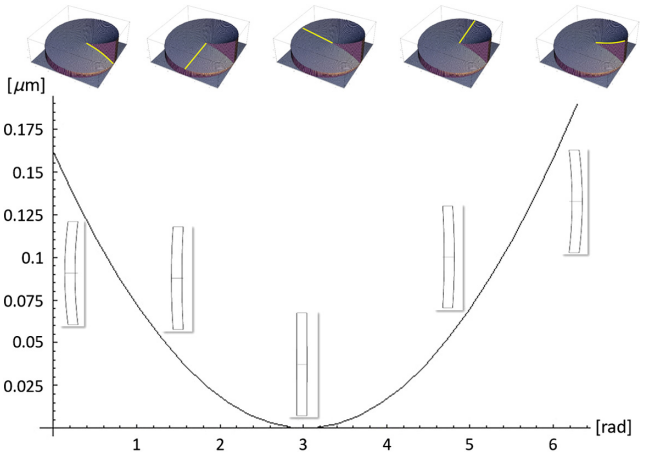

Fig. 5 RMS spot radius versus azimuth and five profile sections of the respective spherical reference lenses in an azimuthal distance of $\pi/2$ as well as the corresponding section lines of the rotation optics.

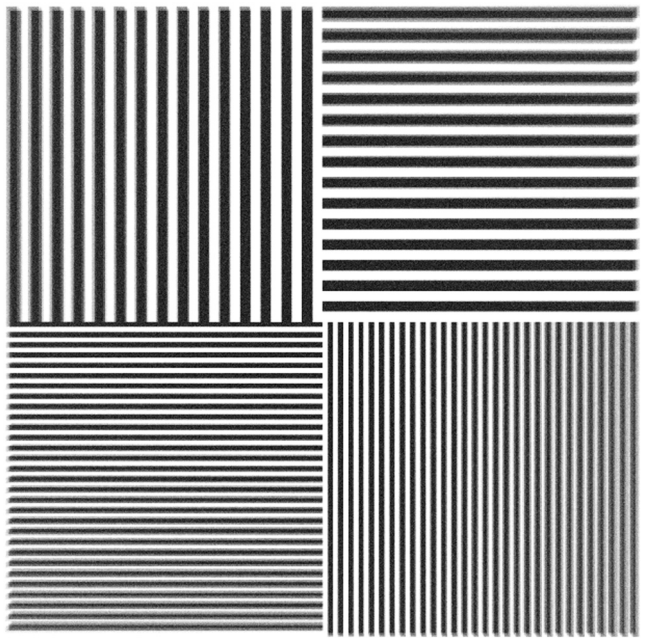

Fig. 6 Geometric image analysis of a line chart. Full field size: 25 deg, calculated rays; 10^8, 1000×1000 pixels.

power of 3 dpt starting with a basic refraction $D_0 = 1$ dpt. To get an impression of how an object will be imaged, a geometric image analysis was conducted using a full field size of 25 deg, 10^8 rays, and 1000×1000 pixels (see Fig. 6). In the peripheral areas, a distortion is clearly visible illustrating the need of further investigations concerning the imaging quality with respect to the field of view. To quantify the image quality Huygens point spread function (PSF) and Strehl ratio were calculated. The object width is infinity; image width depends on the refraction power adjusted. The lens parameters are shown in Fig. 7(a).

Figure 7(b) shows the Huygens PSF and the Strehl ratio in case of a maximum rotation by 45 deg, i.e., for an adjustment of the maximum refraction power of 4 dpt. The diffractive PSF is calculated by OpticStudio using direct integration of the Huygens wavelets method with a pupil sampling (as well as image sampling) of 128×128. This analysis tool is capable of considering diffractive effects as well as aberration effects. The implemented Huygens method accounts for the evolving shape of the diffraction image as the beam propagates to the image surface. This is an important effect if the image surface is tilted with respect to the incoming beam.[34] The Strehl ratio of 1.0 indicates a diffraction-limited performance of the rotation optics for the given parameter set.

Calculating the helical surfaces for larger apertures will increase the amount of spherical aberration and hence will lead to a decrease in performance. Figure 8 shows PSF and Strehl ratio in case of a 20-mm aperture with otherwise the same parameters as shown in Fig. 7(a).

Figure 8 shows a considerable decrease in optical performance due to spherical aberration, which increases its impact with increased aperture. The sensitivity of the performance of the rotation optics due to spherical aberration lies in the fact that all the RMS spot radii for the total azimuth contribute to forming an image (see Fig. 5). To reduce the impact of spherical aberration on the performance, aspherical surfaces were calculated. The aspheres were generated by optimizing both surfaces of the rotation optics to minimize the difference between the RMS spot radii over the azimuth. The surface sag follows Eq. (7), where c is the curvature of the surface and k denotes the conic constant. Optimization of k results in the aspheres desired:

$$z = \frac{cr^2}{1 + \sqrt{1 - (1+k)c^2r^2}} \quad \text{with } r = \sqrt{x^2 + y^2}. \tag{7}$$

Aperture diameter: 5 mm n_L: 1.5 n_0:1.0	
φ_{max}	45 deg
C_0 [mm^{-1}]	-0.024
j [dpt/rad]	7.640

(a)

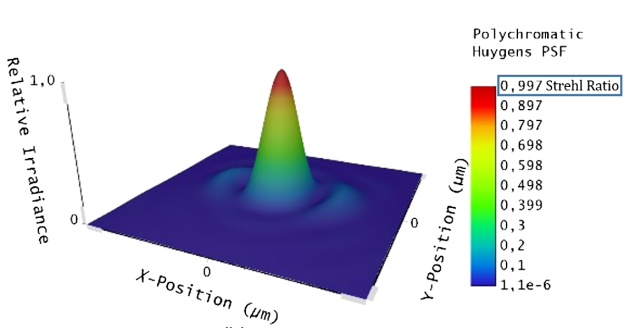

(b)

Fig. 7 (a) Lens parameters) and (b) Huygens PSF and Strehl ratio.

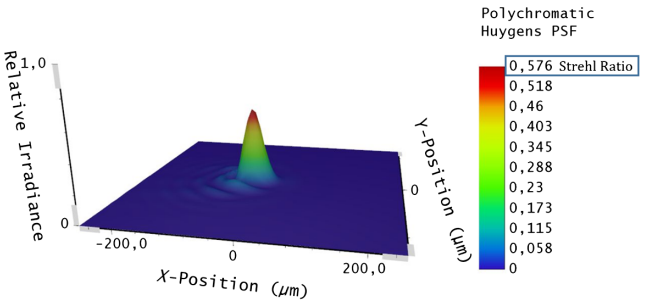

Fig. 8 Huygens PSF and Strehl ratio (right) for 20-mm aperture rotation optics.

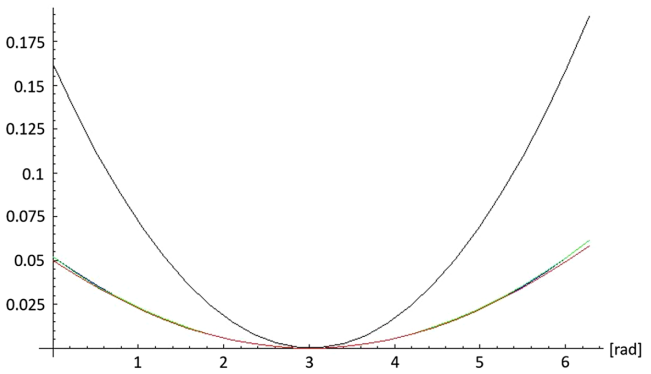

Fig. 9 RMS spot radii versus azimuth: both surfaces spherical (black), first surface aspherical (blue), second surface aspherical (green), and both surfaces aspherical (red).

Figure 9 shows the RMS spot radii over the azimuth in case of both spherical surfaces (black curve, as shown in Fig. 5) and for three different optimization strategies:

- The blue curve in Fig. 9 shows a configuration, where the second surface is still spherical, while the first surface is an optimized asphere to minimize the difference in RMS spot radius for the total azimuth.
- The green curve shows the case, where the first surface remains to be spherical, while the second surface is an asphere.
- And the red line shows the fact where both surfaces are optimized aspheres following Eq. (7).

The surface optimizations were conducted using the state of zero rotation, i.e., the basic refraction power of $D_0 = 1$ dpt. Figure 9 shows a strong improvement of the RMS spot radius using aspheric surfaces. It is also apparent that the difference in performance between the three optimization strategies is only small, hence in the further design process only the first surface is an optimized asphere while the second surface remains spherical. The conic constant $k(\alpha)$ is not independent on the rotation angle φ, i.e., on the adjusted refraction power. Figure 10 shows the optimized conic constant k of the first surface over the azimuth for four different adjustments of refraction power D [$D = 1$ dpt (dot), $D = 2$ dpt (square), $D = 3$ dpt (triangle), and $D = 4$ dpt (diamond)]. Keeping in mind that the transition between concave and convex of the front surface takes place at an azimuth value of $23/24\pi$ (see Fig. 4), it is obvious that for the concave-shaped sector, we experience positive values of the conic constant. Vice versa, above $23/24\pi$, the curvature is convex and the conic constant negative. Also noticeable is the strong spreading of the conic constant for small curvatures (near the transition zone of $23/24\pi$).

The influence of the conic constant on surface shape and hence on the performance is strongly reduced for flat surfaces, i.e., in the region where the spreading of the conic constant is seen to be very large its influence is fortunately negligible. The inset shows details of the interesting part of strongly curved surfaces. Notable is the small spreading of the conic constant for the convex-shaped section while we observe a relative strong spread in case of concave-shaped surfaces. Here again, it can be observed that the spreading increases for decreasing curvatures.

To be able to determine the conic constant in dependence on the azimuth (and independent of the state of rotation), we need to get a functional relationship between the conic

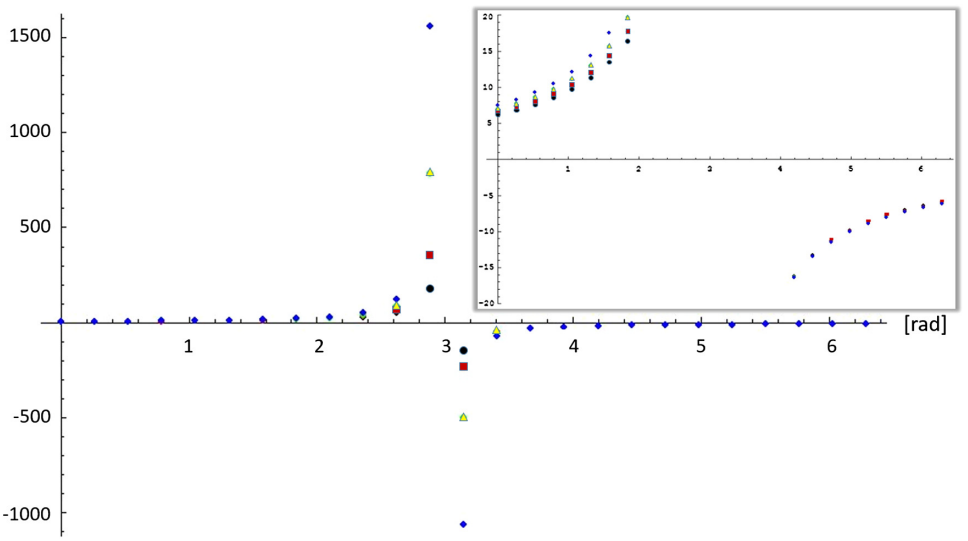

Fig. 10 Optimized conic constant k of the first surface over azimuth: $D = 1$ dpt (dot), $D = 2$ dpt (square), $D = 3$ dpt (triangle), and $D = 4$ dpt (diamond). Inset: detailed representation of strongly curved sectors.

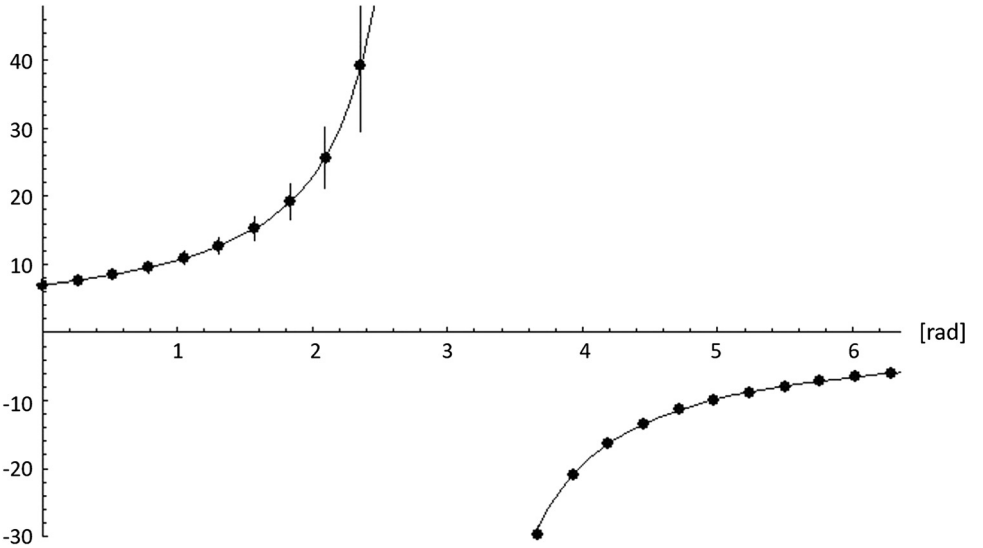

Fig. 11 Averaged conic constants combined with its error bars and the fitted function.

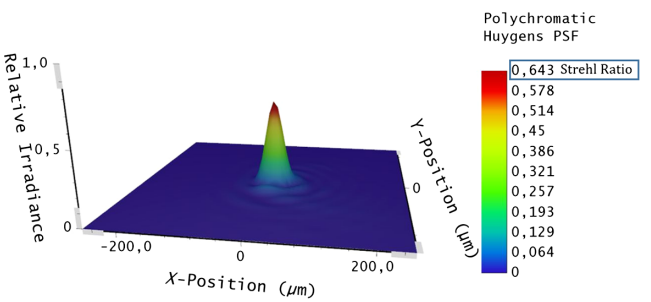

Fig. 12 Huygens PSF and Strehl ratio (right) for 20-mm aperture rotation optics with aspherical surface profiles.

constant and the azimuth. First, an averaging of the conic constant over the four different adjustments of refraction power is performed in dependence on the respective curvature of the front surface. A fit of the mean values will result in a function of the conic constant only depending on the azimuth (i.e., on the curvature), while eliminating the dependence on the rotation angle. The maximum fit error is 5.01×10^{-4}. Figure 11 shows the averaged conic constants in combination with the error bars for averaging and the fitted function.

As expected from the discussion in context of Fig. 10, the error bars increase with increasing conic constant in case of the concave-shaped surfaces. In case of the convex surfaces, the error bars are smaller or at least the same size as the diameter of the dots.

Figure 12 shows the PSF and Strehl ratio for the 20-mm aperture rotation optics with aspherical surface profiles. Comparing the PSF calculated for the aspherical surface (Fig. 12) with that of the spherical surface (Fig. 8) with otherwise same parameters shows a considerable improvement of 12% in optical performance due to the usage of aspherics.

4 Conclusions

We presented a design study of a refractive optics consisting of two lens bodies with helical surface structures. This arrangement allows for tuning the optical refraction power by means of a mutual rotation of the lens bodies around the optical axis. The refraction power of such an optics can be tuned continuously in a defined range. A mathematical description of the helical surface is given for the case of a linear change in curvature. The helical surfaces feature a discontinuity at the transition from $\alpha = 2\pi$ to $\alpha = 0$. Since this discontinuity will seriously affect the imaging quality, it has to be obscured to prevent any adverse effects in imaging, such as, e.g., scattering. Rotation of the optics forms two sectors with different, tunable refraction power resulting in a tunable multifocal optics where the difference ΔD between both sectors is a constant depending on the refraction indices of the materials used and the linear factor k. To form a monofocal optics, the undesired sector has to be obscured.

An exemplary design of such an optics with an amplitude of refraction power of 3 dpt and an optical-free aperture of 5 mm shows an almost diffraction limited optical performance. Increasing the free aperture leads to an increase of the impact of spherical aberration, hence the optical performance is decreased noticeably. To compensate for spherical aberration effects, an approach to calculating aspherical surface profiles was developed and exemplarily compared to rotation optics based on spherical surface profiles in case of an aperture of 20 mm. As a result, an improvement of the Strehl ratio of 12% was shown. A strong correlation between the aperture size of the rotation optics and aberration effects are evident as well as a correlation between the maximum rotation angle and aberrations. The investigation of optical power limitations of rotation optics as well as quantification of its performance limits is the basis of our resent research. Quantification of these relationships and the limitations as well as promising compensations are currently under investigation.

References

1. F. Z. Fang et al., "Manufacturing and measurement of free-form optics," *CIRP Ann.* **62**(2), 823–846 (2013).
2. J. D. Owen et al., "On the ultraprecision diamond machining of chalcogenide glass," *CIRP Ann.* **64**, 113–116 (2015).
3. L. Li et al., "Fabrication of microinjection molded miniature freeform Alvarez lenses," *Appl. Opt.* **53**(19), 4248–4255 (2014).
4. L. Li et al., "Design and fabrication of microinjection molded miniature freeform Alvarez lenses," in *Proc. ASPE/ASPEN Summer Topical*

Meeting: Manufacture and Metrology of Freeform and Off-Axis Aspheric Surfaces, pp. 13–16 (2014).
5. F. Chen et al., "Design method of high-efficient LED headlamp lens," *Opt. Express* **18**, 20926–20938 (2010).
6. C. Hsieh, Y. Li, and C. Hung, "Modular design of the LED vehicle projector headlamp system," *Appl. Opt.* **52**, 5221–5229 (2013).
7. F. Duerr and H. Thienpont, "Analytic design of a zoom XY-beam expander with free-form optical surfaces," *Opt. Express* **23**, 30438–30447 (2015).
8. Y. Schwartzburg et al., "High-contrast computational caustic design," *ACM Trans. Graphics* **33**, 74 (2014).
9. T. Kiser and M. Pauly, "Caustic art," No. EPFL-REPORT-196165 (2012).
10. T. Kiser et al., "Architectural caustics—controlling light with geometry," in *Advances in Architectural Geometry*, L. Hesselgren et al., Eds., pp. 91–106, Springer, Vienna (2012).
11. L. W. Alvarez, "Two-element variable-power spherical lens," U.S. Patent 3305294 (1964).
12. A. W. Lohmann, "A new class of varifocal lenses," *Appl. Opt.* **9**(7), 1669–1671 (1970).
13. L. W. Alvarez, "Development of variable-focus lenses and new refractor," *J. Am. Optom. Assoc.* **49**(1), 24–29 (1978).
14. S. Barbero, "The Alvarez and Lohmann refractive lenses revisited," *Opt. Express* **17**(11), 9376–9390 (2009).
15. S. Barbero and J. Rubinstein, "Adjustable-focus lenses based on the Alvarez principle," *J. Opt.* **13**(12), 125705 (2011).
16. S. S. Rege, T. S. Tkaczyk, and M. R. Descour, "Application of the Alvarez–Humphrey concept to the design of a miniaturized scanning microscope," *Opt. Express* **12**(12), 2574–2588 (2004).
17. I. A. Palusinski, J. M. Sasian, and J. E. Greivenkamp, "Lateral-shift variable aberration generators," *Appl. Opt.* **38**(1), 86–90 (1999).
18. S. Barbero and J. Rubinstein, "Power-adjustable sphero-cylindrical refractor comprising two lenses," *Opt. Eng.* **52**(6), 063002 (2013).
19. I. Sieber et al., "Optical performance simulation of free-form optics for an eye implant based on a measurement data enhanced model," *Appl. Opt.* **55**(24), 6671–6679 (2016).
20. I. Sieber et al., "Optical design and tolerancing of an ophthalmological system," *Proc. SPIE* **9195**, 919504 (2014).
21. A. N. Simonov, G. Vdovin, and M. C. Rombach, "Cubic optical elements for an accommodative intraocular lens," *Opt. Express* **14**(17), 7757–7775 (2006).
22. I. Sieber, T. Martin, and U. Gengenbach, "Robust design of an optical micromachine for an ophthalmic application," *Micromachines* **7**(5), 85 (2016).
23. S. Bernet and M. Ritsch-Marte, "Adjustable refractive power from diffractive moiré elements," *Appl. Opt.* **47**(21), 3722–3730 (2008).
24. S. Bernet, W. Harm, and M. Ritsch-Marte, "Demonstration of focus-tunable diffractive Moiré-lenses," *Opt. Express* **21**(6), 6955–6966 (2013).
25. W. Harm et al., "Adjustable diffractive spiral phase plates," *Opt. Express* **23**(1), 413–421 (2015).
26. S. F. Busch et al., "Extending the Alvarez-lens concept to arbitrary optical devices: tunable gratings, lenses, and spiral phase plates," *IEEE Trans. Terahertz Sci. Technol.* **7**(3), 320–325 (2017).
27. A. Grewe, P. Fesser, and S. Sinzinger, "Diffractive array optics tuned by rotation," *Appl. Opt.* **56**(1), A89–A96 (2017).
28. T. Martin et al., "Lens system having adjustable refraction strength," WO 2013/041222 A1 (2013).
29. I. Sieber, T. Martin, and P. Stiller, "Tunable refraction power by mutual rotation of helical lens parts," *Proc. SPIE* **10375**, 103750L (2017).
30. I. Sieber et al., "Design-for-manufacture of a varifocal rotation optics," *Proc. SPIE* **10690**, 106901B (2018).
31. G. Bretthauer, U. Gengenbach, and R. F. Guthoff, "Mechatronic systems to restore accommodation," in *Nova Acta Leopold*, pp. 167–175 (2010).
32. OpticStudio, https://www.zemax.com/products/opticstudio (27 March 2018).
33. Mathematica, https://www.wolfram.com/mathematica/ (27 March 2018).
34. OpticStudio 16.5 SP4, "Help files," April 2017, pp. 915–920 (2017).

Ingo Sieber received his PhD from the University of Bremen in 1999 and his habilitation in 2016 from Karlsruhe Institute of Technology (KIT). Since 2001, he focuses his works on "system integration: modeling and simulation" at the Institute for Automation and Applied Informatics (IAI) of KIT. His main research interests are interdomain simulations of nano- and microsystems as well as design-for-manufacturing and robust design of optical subsystems and systems.

Peter Stiller received his diploma in mathematics from the University of Karlsruhe in 1981. Since then he has been with the IAI of KIT, doing software development.

Ulrich Gengenbach received his PhD degree in 1992 and his habilitation in 2018 both from the University of Karlsruhe. He is head of the research area "system integration for micro- and nano-systems" at the IAI of KIT. His main research interests are methodical design of and integration technologies for nano- and microsystems.